Research Square

Preprints are preliminary reports that have not undergone peer review.
They should not be considered conclusive, used to inform clinical practice,
or referenced by the media as validated information.

Efficient Analytical Modeling of Gravitational Fields of Irregular Asteroids: Applications to Lutetia, Bennu, Apophis, Itokawa, and Sylvia

Marcelo Lisboa Mota

prof.mlmota@ifsp.edu.br

Federal Institute of São Paulo

Safwan Aljbaae

University of Atacama

Antonio F. B. Almeida Prado

Instituto Nacional de Pesquisas Espaciais

Allan Kardec de Almeida

University of Coimbra

Article

Keywords: Astrodynamics, gravity potential, asteroids, equilibrium points, stability

Posted Date: July 22nd, 2026

DOI: https://doi.org/10.21203/rs.3.rs-10036312/v1

License: This work is licensed under a Creative Commons Attribution 4.0 International License.
Read Full License

Additional Declarations: No competing interests reported.

Efficient Analytical Modeling of Gravitational Fields of Irregular Asteroids: Applications to Lutetia, Bennu, Apophis, Itokawa, and Sylvia

Marcelo L. Mota[1*], Safwan Aljbaae[2*], Antonio F. B. A. Prado[3] and Allan K. de Almeida Jr.[4]

[1]Federal Institute of São Paulo, IFSP, Avenida Thereza Ana Cecon Breda, s/n - Vila São Pedro, Hortolândia, 13183-250, SP, Brazil.
[2]Instituto de Astronomía y Ciencias Planetarias - INCT, Universidad de Atacama-UDA, Copayapu 485, Copiapó 1531772, Chile.
[3]Post Graduate Division, INPE, Av. dos Astronautas, 1.758 - Jardim da Granja, São Jose dos Campos, 12227-010, São Paulo, Brazil.
[4]CFisUC, Departamento de Física, Universidade de Coimbra, Coimbra, 3004-516, Portugal.

*Corresponding author(s). E-mail(s): prof.mlmota@ifsp.edu.br; safwan.aljbaae@gmail.com;

Abstract

This study aims to create efficient analytical models for the gravitational fields of several asteroids: (21) Lutetia, (101955) Bennu, (99942) Apophis, (25143) Itokawa, and (87) Sylvia. For this purpose, we establish an analytical model that reproduces the gravitational field around non-spherical bodies with constant density, while also allowing the analysis of modeling effects when considering bodies composed of multiple layers and, therefore, different densities. Due to the non-spherical geometry of such bodies, their gravitational potential deviates from a central field. By representing the body as a polyhedron and decomposing it into tetrahedral elements, we apply the Series Potential Expansion Method (PSEM) to approximate the total potential by summing the contributions of each tetrahedron.

Our results show that, although this model does not provide higher accuracy than the classical polyhedral approach, it achieves relative errors below 0.1% for points

outside the body when developed to higher orders (e.g., orders 11 and 12). On the other hand, the model proposed in this paper significantly reduces execution time, thereby improving computational efficiency. We determine equilibrium points, analyze their stability, investigate zero-velocity planes, and compute the relative errors between the gravitational field modeled by PSEM and those obtained using both the classical polyhedral method of Tsoulis and Petrović and the mass concentration method.
These results demonstrate the computational efficiency of the proposed approach for modeling the gravitational potential of irregularly shaped bodies. The model provides a robust framework for more complex analyses, such as the study of periodic orbits around non-spherical celestial bodies, stability assessments, and the planning of smooth spacecraft landing trajectories. Furthermore, this technique can be extended to other irregular bodies.

Keywords: Astrodynamics, gravity potential, asteroids, equilibrium points, stability

1 Introduction

Today, examining the behavior of objects near asteroids is essential for planetary defense, resource extraction, mission planning, and many other reasons. Asteroids possess irregular shapes because their mass is insufficient for gravity to overcome the internal structural strength of their material. Consequently, they cannot achieve the hydrostatic equilibrium required to form a smooth sphere, as planets or larger moons do. This renders their gravitational environment complicated to model with reasonable accuracy for long-term perturbation effects. Such complexity significantly affects spacecraft orbits, along with forces such as solar radiation pressure and solar tides. Consequently, developing accurate gravity formulations is critical for trajectory planning, stability evaluation, and mission safety. On the other hand, when available, accurate potential modeling is usually computationally expensive.

Several strategies have been developed to precisely predict the gravitational field of irregular tiny entities. Each offering trade-offs among accuracy, computing effort, and application. Classical spherical-harmonic expansions, introduced by MacMillan [1] and later refined by Kaula [2], Heiskanen and Moritz [3], Balmino [4], Roithmayr [5], Casotto [6], provide a closed-form external field representation, but are only viable outside the Brillouin sphere. Near the surface of strongly irregular bodies, truncated expansions may diverge or require high degrees, compromising stability and computational efficiency [7]. To overcome these limitations, the polyhedral method of Werner [8] offers an exact analytical solution for homogeneous bodies through integrated face and edge contributions. Although highly accurate and used operationally [9], the solid-angle and projection terms involved may become numerically sensitive when the evaluation point lies close to the surface.

To improve robustness in such regions, Tsoulis reformulated the polyhedral field using closed-form line and surface integrals expressed through logarithmic and arctangent functions. This formulation normalizes the contributions of faces, edges, and vertices, preserving continuity and removing singularities even when the field point coincides with the surface [10, 11]. Although this formulation resolves numerical singularities and improves close-proximity robustness, it does so at the cost of significantly increased computational effort, since its closed-form expressions involve repeated evaluations of trigonometric functions, logarithmic terms, and geometric transformations for every face and edge.

Mascon-based alternatives also exist, substituting the mass distribution with point masses [12], but they often lack geometric fidelity. Later refinements introduced polyhedral-source mascon models by decomposing the volume into tetrahedra and positioning point masses at their barycenters, preserving shape accuracy and allowing density layering [13, 14]. Other research revealed the superior fidelity of polyhedral gravity near the surface in comparison to mascon-based methods [15].

In recent years, data-driven techniques have also emerged as complementary solutions. GeodesyNets [16] and PINN-based gravity models [17] show that machine learning Neural techniques can minimize model error at the surface and overcome truncated expansion restrictions. However, such data-driven techniques are heavily reliant on the distribution and quality of training data, which is sometimes limited for irregular or concave asteroids. These models may smooth out essential features or extrapolate poorly outside the training region.

Within this landscape, we have been developing the Potential Series Expansion Method (PSEM) [18], which combines power-series expansion with tetrahedral volume discretization. By expanding the potential of each tetrahedral element and summing contributions, PSEM provides a convergent analytical representation outside the Brillouin sphere [19]. Its closed-form structure also enables efficient evaluation of potentials, gradients, and higher-order terms, significantly reducing computational cost while maintaining close agreement with classical polyhedral models [20]. In fact, application to (87) Sylvia demonstrated the accuracy and efficiency of PSEM when compared with layered mascon and polyhedral methods.

However, the present manuscript advances beyond previous contributions by demonstrating its performance across several other asteroids, including cases with distinct internal density structures. Furthermore, we derive explicit analytical expressions for the gravitational potential of these celestial bodies. For this purpose, we numerically evaluate the coefficients of the polynomial expansion based on the PSEM. The results show remarkable efficiency, with substantial computational gains and a reasonable loss of accuracy when compared with the potential derived using the classical polyhedral technique [10].

Assuming a homogeneous or layered-density structure, rigid-body rotation at constant rate, and negligible external perturbations, Section 2 presents the governing

formulation of PSEM. Section 3 describes the computational framework. Section 4 applies the method to a set of representative irregular asteroids and compares the results with classical polyhedral solutions, including cases with internal stratification. Section 5 concludes with a discussion and implications for gravity modeling in small-body environments.

2 Potential series expansion method

In this section, we present the mathematical development of the Potential Series Expansion Method (PSEM) [18] to model the gravitational field around an asteroid, assuming a homogeneous density. We only consider the gravitational field itself, leaving other perturbations, such as solar radiation pressure, the Sun's gravitational influence, and additional forces, for future studies.

2.1 Uniform-Density Gravitational Field Modeling

Consider a Cartesian inertial coordinate system (X_I, Y_I, Z_I), in which (X_o, Y_o, Z_o) denote the coordinates of the center of mass O of a body Q, and $(\overline{X}, \overline{Y}, \overline{Z})$ the coordinates of a particle of mass m located at point P. Now introduce a new coordinate system (ξ, η, ζ) fixed to the body, with origin at its center of mass and axes parallel to those of the inertial system. Let dm be a mass element of the body Q, located at point B with coordinates (ξ, η, ζ) in the body-fixed system, as illustrated in Figure 1.

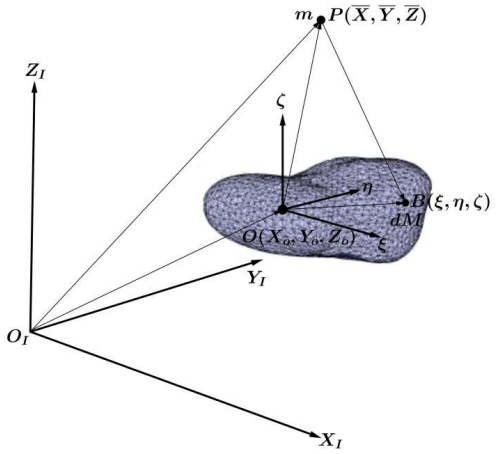


Fig. 1 Coordinate Systems for Calculating Gravitational Force.

Defining $(x,\ y,\ z)$ as the coordinates of m relative to the coordinate system fixed to the body, we obtain Equation (1).

$$x = \overline{X} - X_o, \qquad y = \overline{Y} - Y_o, \qquad z = \overline{Z} - Z_o, \tag{1}$$

Consequently, the distance r between points P and B is given by Equation (2).

$$r^2 = (x-\xi)^2 + (y-\eta)^2 + (z-\zeta)^2. \tag{2}$$

Now, using the fundamental tools developed by Kellogg [21] and MacMillan [1], together with the polyhedral decomposition method introduced by Werner [8], we aim to present a methodology for approximately calculating the potential of a body with an asymmetric mass distribution. To achieve this, we compute the potential of each tetrahedron, so that the total potential of the polyhedron is obtained as the sum of the individual tetrahedral contributions.

In this first study, consider a homogeneous solid with a non-spherical mass distribution Q, whose center of mass is located at the origin of the body-fixed coordinate system with Cartesian coordinates (ξ, η, ζ). Similar to the polyhedral method developed by Werner and Scheeres [7], it is necessary to model the shape of this solid as a polyhedron by adding tetrahedral elements. This is accomplished by connecting the vertices of the triangular facets on its surface to its center of mass, as illustrated in Figure 2.

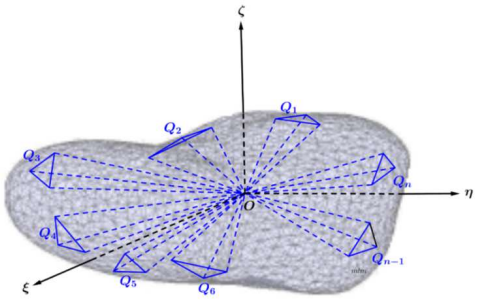


Fig. 2 Homogeneous solid Q with non-spherical geometry decomposed into tetrahedra.

Let Q_k be a generic tetrahedron of mass M_k, formed by the vertices V_{1_k}, V_{2_k}, V_{3_k}, and O, with the latter positioned at the origin of the Cartesian coordinate system (ξ, η, ζ), as illustrated in Figure 3.

Consider a unit mass at a point $P(x, y, z)$ and an element of mass dM at any point inside the tetrahedron Q_k, denoted as $B(\xi, \eta, \zeta)$. Defining γ as the angle between the vectors $\overrightarrow{OP}$ and $\overrightarrow{OB}$, and using the cosine theorem, one can obtain the value of r as

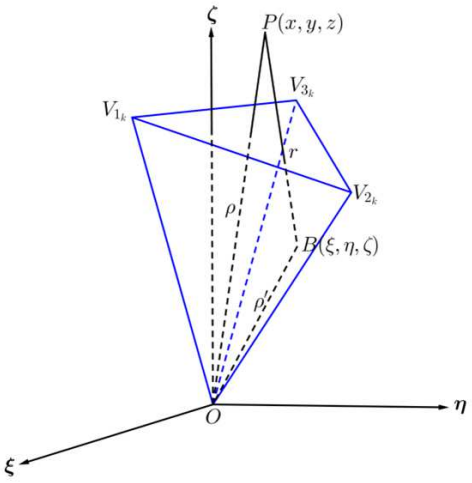


Fig. 3 Tetrahedron Q_k with vertices V_{1_k}, V_{2_k}, V_{3_k}, and O.

shown in Equation (3).

$$r^2 = \rho^2 + \rho'^2 - 2\rho\rho' \cos\gamma. \tag{3}$$

Isolating $\frac{1}{r}$ from Equation (3), we obtain Equation (4).

$$\frac{1}{r} = \frac{1}{\sqrt{\rho^2 + \rho'^2 - 2\rho\rho' \cos\gamma}}, \tag{4}$$

and factoring out ρ^2, we obtain Equation (5).

$$\frac{1}{r} = \frac{1}{\rho\sqrt{1 - 2\frac{\rho'}{\rho}\cos\gamma + \frac{\rho'^2}{\rho^2}}}. \tag{5}$$

Defining $\chi = \rho'/\rho$ and $u = \cos\gamma$, Equation (5) becomes Equation (6)

$$\frac{1}{r} = \frac{1}{\rho\sqrt{1 - 2\chi u + \chi^2}} \tag{6}$$

.

Expanding the function $\left(\sqrt{1 - 2u\chi + \chi^2}\right)^{-1}$ into a convergent power series in χ, we obtain Equation (7).

$$\frac{1}{\sqrt{1 - 2u\chi + \chi^2}} = \sum_{i=0}^{m} P_i(u)\,\chi^i \tag{7}$$

provided that $|\chi| < \sqrt{2} - 1$, with $P_0(u)$, $P_1(u)$, $P_2(u), \ldots$ being the corresponding Legendre polynomials. Thus, Equation (7) can be written as a series of negative powers of the variable ρ in Equation (8).

$$\frac{1}{r} = P_o\left(u\right)\frac{1}{\rho} + P_1\left(u\right)\frac{\rho'}{\rho^2} + P_2\left(u\right)\frac{\rho'^2}{\rho^3} + \ldots \tag{8}$$

It is worth noting that the series given by Equation (8) converges uniformly for any point P outside the Brillouin sphere, that is, the smallest sphere that encompasses all the mass of the body, ensuring reliable approximations of the gravitational field. However, within this sphere, similarly to the spherical harmonic method, the series may diverge.

Thus, considering the interval of convergence and assuming that the density of the solid is constant, $\sigma = M_k/V_k$ (with the possibility of extending the analysis to bodies composed of three layers), the term-by-term integration of Equation (8) over the volume of the solid Q_k yields a series expansion of the potential associated with the mass distribution of each tetrahedron, represented by $U^{(k)}$, as given in Equation (9).

$$U^{(k)} = G\sigma \sum_{i=0}^{\infty} \iiint_{Q_k} P_i\left(u\right)\frac{\rho'^i}{\rho^{i+1}} dV \tag{9}$$

where $dV = d\xi\, d\eta\, d\zeta$ and $G = (6.6742 \pm 0.0010) \times 10^{-11}\,\mathrm{m^3\,kg^{-1}\,s^{-2}}$ is the gravitational constant. In this way, rewriting Equation (9) appropriately gives us Equation (10).

$$U^{(k)} = G\sigma \sum_{i=0}^{\infty} \iiint_{Q_k} P_i\left(u\right)\frac{\rho'^i\rho^i}{\rho^{2i+1}} dV\,. \tag{10}$$

Equation (10) should be truncated to obtain an approximate potential for the tetrahedron Q_k, as shown in Equation (11):

$$U^{(k)} = G\sigma \sum_{i=0}^{m} \iiint_{Q_k} P_i\left(u\right)\frac{\rho'^i\rho^i}{\rho^{2i+1}} dV + \varepsilon_k \tag{11}$$

where m is the degree of the developed potential and ε_k is the associated truncation error. It is worth noting that the larger the value of m, the smaller ε_k becomes, balancing computational cost with precision. Furthermore, from Figure 3, with $u =$

$\cos\gamma$ denoting the angle between the vectors $\overrightarrow{OP}$ and $\overrightarrow{OB}$, $\rho = \sqrt{x^2+y^2+z^2}$, and $\rho' = \sqrt{\xi^2+\eta^2+\zeta^2}$, we obtain Equation (12).

$$u\rho\rho' = \xi x + \eta y + \zeta z. \tag{12}$$

Thus, substituting the Legendre polynomials $P_i(u)$, ρ, and ρ', and considering Equation (12), each integrand in Equation (11) becomes a homogeneous polynomial function in the variables (ξ, η, ζ). Therefore, the determination of the potential is tied to evaluating the integral expressions in Equation (11), which can be simplified using the method developed by Lien and Kajiya [22]. This symbolic method is fundamental to our approach, as it establishes a linear transformation (isometry) between the points of a generic tetrahedron and those of a rectangular tetrahedron, both having one vertex at the origin of their respective coordinate systems. This transformation resolves the main difficulty in calculating triple integrals over a generic tetrahedron—namely, determining the limits of integration. By transforming to a rectangular tetrahedron, these limits become well-defined and substantially simplified.

The method also utilizes the Beta and Gamma functions, well established in mathematical physics, as detailed in Appendix A, as well as the relationships between these functions, which are essential for streamlining the triple integral calculation. The result of this integral is then multiplied by the Jacobian determinant of the transformation matrix to map the solution back to the original coordinate system. This procedure yields the value of the potential generated by a generic tetrahedron. By summing the contributions of all tetrahedra, the total gravitational potential of the polyhedron is obtained.

We observe that the coordinate system is fixed to the polyhedron (asteroid), with the origin located at the center of mass and the axes aligned with the principal axes of inertia. This configuration ensures consistency in our calculations across all tetrahedra that comprise the polyhedron. This combination of geometric and mathematical simplifications is a cornerstone of the Potential Series Expansion Method (PSEM) and is fundamental to its efficiency and accuracy. For additional details on the symbolic method and its applications, consult Mota [18].

The integrands of Equation (11) are polynomials represented generically by Equation (13).

$$f(\xi,\eta,\varsigma) = \sum_{n_1,n_2,n_3} \xi^{n_1}\eta^{n_2}\zeta^{n_3}, \tag{13}$$

where the indices n_1, n_2, and n_3 denote the powers of the variables ξ, η, and ζ in the polynomial expansion. The sum is performed over all combinations of these indices, up to the specified order of expansion, allowing for an accurate approximation of the

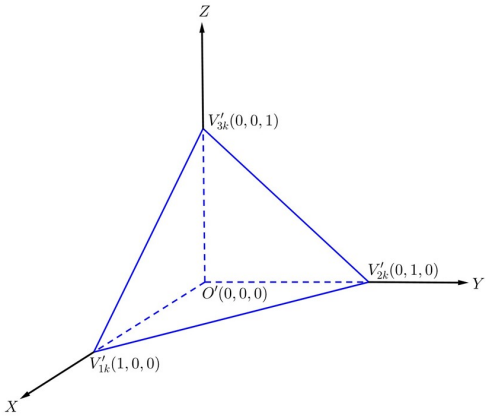


Fig. 4 Tetrahedron W with vertices V'_{1_k}, V'_{2_k}, V'_{3_k}, and O.

gravitational potential.

To evaluate the integrals appearing in Equation (11), we focus our attention on the generic integral given by Equation (14).

$$I = \iiint_{Q_k} \xi^{n_1} \eta^{n_2} \zeta^{n_3} d\xi d\eta d\zeta. \tag{14}$$

Assuming the tetrahedron vertices in Figure 3 are $O(0,0,0)$, $V_{1_k}\,(\xi_{1_k}, \eta_{1_k}, \zeta_{1_k})$, $V_{2_k}\,(\xi_{2_k}, \eta_{2_k}, \zeta_{2_k})$, and $V_{3_k}\,(\xi_{3_k}, \eta_{3_k}, \zeta_{3_k})$, the linear transformation T is expressed by Equation (15).

$$T = \begin{pmatrix} \xi_{1_k} & \xi_{2_k} & \xi_{3_k} \\ \eta_{1_k} & \eta_{2_k} & \eta_{3_k} \\ \zeta_{1_k} & \zeta_{2_k} & \zeta_{3_k} \end{pmatrix}. \tag{15}$$

This establishes an isometry between the coordinate system (ξ, η, ζ) and the new system (X, Y, Z), as shown in Equation (16).

$$\begin{pmatrix} \xi \\ \eta \\ \zeta \end{pmatrix} = \begin{pmatrix} \xi_{1_k} & \xi_{2_k} & \xi_{3_k} \\ \eta_{1_k} & \eta_{2_k} & \eta_{3_k} \\ \zeta_{1_k} & \zeta_{2_k} & \zeta_{3_k} \end{pmatrix} \begin{pmatrix} X \\ Y \\ Z \end{pmatrix}, \tag{16}$$

transforming the initial tetrahedron into a rectangular tetrahedron whose vertices are $O'(0,0,0)$, $V'_{1k}(1,0,0)$, $V'_{2k}(0,1,0)$, and $V'_{3k}(0,0,1)$, as shown in Figure 4.

According to the transformation given in Equation (16), the integral in Equation (14) can be rewritten as shown in Equation (17).

$$I = ||T|| \iiint_W \tilde{X}^{n_1} \tilde{Y}^{n_2} \tilde{Z}^{n_3} dX\, dY\, dZ. \tag{17}$$

where $\tilde{X} = \xi_{1k}X + \xi_{2k}Y + \xi_{3k}Z$, $\tilde{Y} = \eta_{1k}X + \eta_{2k}Y + \eta_{3k}Z$, and $\tilde{Z} = \zeta_{1k}X + \zeta_{2k}Y + \zeta_{3k}Z$, while $\|T\|$ denotes the Jacobian determinant of the transformation matrix.

Evaluating the integral of a generic polynomial function of the form $X^{n_1}Y^{n_2}Z^{n_3}$ over the rectangular tetrahedron, we obtain Equation (18).

$$\int_0^1 \int_0^{1-Z} \int_0^{1-Y-Z} X^{n_1} Y^{n_2} Z^{n_3} dX dY dZ = \frac{n_1!\, n_2!\, n_3!}{(n_1 + n_2 + n_3 + 3)\,!}. \tag{18}$$

Thus, Equation (17) represents the integral expressed in the transformed coordinate system, while Equation (18) presents the simplified result of this same integral over the rectangular tetrahedron in the original coordinate system. This procedure ensures a smooth transition between the two formulations and highlights the efficiency of the method.

Therefore, the potential function of the non-spherical solid $Q = \bigcup_{k=1}^{n} Q_k$, with n being the total number of tetrahedra forming the polyhedron Q, relative to the unit mass located at point $P(x, y, z)$, is given by Equation (19).

$$U^{(m)} = G\sigma \sum_{k=1}^{n} \sum_{i=0}^{m} \iiint_{Q_k} P_i(u) \frac{\rho'^i \rho^i}{\rho^{2i+1}} dV + \varepsilon = G\sigma \sum_{i=0}^{m} \iiint_{Q} P_i(u) \frac{\rho'^i \rho^i}{\rho^{2i+1}} dV + \varepsilon, \tag{19}$$

where $\varepsilon = \sum_{k=1}^{n} \varepsilon_k$ and m is the degree of the calculated potential.

To exemplify the application of the potential series expansion method, and assuming that the body Q is homogeneous, we describe the assembly of some of the integrands of Equation (19). Thus, knowing that $P_0(u) = 1$, the calculation of the zero-degree potential is given by Equation (20).

$$U_0 = G\sigma \sum_{k=1}^{n} \iiint_{Q_k} P_o(u) \frac{1}{\rho} dV = G\frac{M}{V} \frac{1}{\rho} \sum_{k=1}^{n} \iiint_{Q_k} dV = \frac{GM}{\rho}, \tag{20}$$

which represents the Keplerian potential. Similarly, by considering only the second term of the sum given in Equation (19), with $P_1(u) = u$, we obtain Equation (21).

$$U_1 = G\frac{M}{V}\iiint\limits_Q P_1(u)\,\frac{\rho'\rho}{\rho^3}dV = \frac{GM}{\rho^3\,V}\iiint\limits_Q (u\rho'\rho)\;dV, \tag{21}$$

and taking into account that $u\rho\rho' = \xi x + \eta y + \zeta z$, the first-degree potential is then given by Equation (22).

$$U_1 = \frac{GM}{\rho^3\,V}\iiint\limits_Q (x\xi + y\eta + z\zeta)\;dV, \tag{22}$$

whose result is $U_1 = 0$, since the origin of the coordinate system fixed to the asteroid coincides with its center of mass. Following the same reasoning, the third term of the sum in Equation (19), with $P_2(u) = \frac{1}{2}\left(3u^2 - 1\right)$, corresponding to the degree-2 potential, is given by Equation (23).

$$U_2 = G\frac{M}{V}\iiint\limits_Q P_2(u)\,\frac{\rho'^2\rho^2}{\rho^5}dV = G\frac{M}{\rho^5 V}\iiint\limits_Q \left[\frac{3}{2}(u\rho'\rho)^2 - \frac{1}{2}\rho'^2\rho^2\right]dV \tag{23}$$

and, since $\rho = \sqrt{x^2+y^2+z^2}$ and $\rho' = \sqrt{\xi^2+\eta^2+\zeta^2}$, the potential of degree two is given by Equation (24).

$$U_2 = \frac{GM}{\rho^5\,V}\iiint\limits_Q \left[\frac{3}{2}(x\xi + y\eta + z\zeta)^2 - \frac{1}{2}\left(\xi^2+\eta^2+\zeta^2\right)\left(x^2+y^2+z^2\right)\right]dV, \tag{24}$$

in which the coefficients of the terms in xy, xz, and yz are zero, since the axes of the fixed system coincide with the principal axes of inertia, as initially established. Similarly, the fourth term of the sum in Equation (19), that is, the potential of degree 3, with $P_3(u) = \frac{1}{2}\left(5u^3 - 3u\right)$, is expressed by Equation (25).

$$U_3 = G\frac{M}{V}\iiint\limits_Q P_3(u)\,\frac{\rho'^3\rho^3}{\rho^7}dV = G\frac{M}{\rho^7 V}\iiint\limits_Q \left[\frac{5}{2}(u\rho'\rho)^3 - \frac{3}{2}(u\rho'\rho)\,\rho'^2\rho^2\right]dV. \tag{25}$$

Following the evaluation of the integrals over the solid Q shown above for each term U_l with $l \in [\![0 : m]\!]$, the potential given in Eq. (19) can be written in polynomial terms as

$$U = \sum_{l=0}^{m} \sum_{i,j,k=0}^{l} U_l^{i,j,k} x^i y^j z^k (x^2 + y^2 + y^2)^{-\frac{2l+1}{2}} + \varepsilon \ \forall i, j, k, l \in \mathbb{N} : i + j + k = l \quad (26)$$

In order to provide a clearer visualization to the reader, the first sum in Eq. (26) can be represented as

$$U = U_0 + U_1 + U_2 + U_3 + ... + U_m + \varepsilon, \quad (27)$$

where U_0 is the Keplerian potential, while the sum of the remaining terms represents the perturbation due to the non-central gravitational field through higher-degree terms. For instance, the first four terms on the right-hand side of Eq. (27) can be expanded as

$$\begin{aligned}
U_0 &= \frac{U_0^{0,0,0}}{r} \\
U_1 &= \frac{U_1^{1,0,0} x}{r^3} + \frac{U_1^{0,1,0} y}{r^3} + \frac{U_1^{0,0,1} z}{r^3} \\
U_2 &= \frac{U_2^{2,0,0} x^2}{r^5} + \frac{U_2^{1,1,0} xy}{r^5} + \frac{U_2^{0,2,0} y^2}{r^5} + \frac{U_2^{1,0,1} xz}{r^5} + \frac{U_2^{0,1,1} yz}{r^5} + \frac{U_2^{0,0,2} z^2}{r^5} \\
U_3 &= \frac{U_3^{3,0,0} x^3}{r^7} + \frac{U_3^{2,1,0} x^2 y}{r^7} + \frac{U_3^{1,2,0} xy^2}{r^7} + \frac{U_3^{0,3,0} y^3}{r^7} + \frac{U_3^{2,0,1} x^2 z}{r^7} + \frac{U_3^{1,1,1} xyz}{r^7} \\
&\quad + \frac{U_3^{0,2,1} y^2 z}{r^7} + \frac{U_3^{1,0,2} xz^2}{r^7} + \frac{U_3^{0,1,2} yz^2}{r^7} + \frac{U_3^{0,0,3} z^3}{r^7},
\end{aligned} \quad (28)$$

where $r = \sqrt{x^2 + y^2 + z^2}$.

2.2 Three-Layer Asteroid Gravity Model with Variable Densities

In the previous subsection, we modeled the potential of an asteroid assuming its density to be constant. Let us now consider the same asteroid, but with an internal structure composed of three concentric layers, each with a different density, such that the average density remains equal to the homogeneous case. With this procedure, the mass distribution is modified to reflect a higher concentration toward the center of the asteroid while keeping its total mass constant. To describe the procedure, we take a tetrahedral element and divide it into three volumes with parallel bases $A_1B_1C_1$, $A_2B_2C_2$, and $A_3B_3C_3$, as shown in Figure 5.

To compute the total potential of the tetrahedral element Q_k shown in Figure 5, we consider each layer with its corresponding density. Defining $U_{t_1\sigma_1}^{(k)}$ as the potential of tetrahedron $OA_1B_1C_1$ with density σ_1, $U_{t_2\sigma_1}^{(k)}$ as the potential of tetrahedron $OA_2B_2C_2$ with density σ_1, $U_{t_2\sigma_2}^{(k)}$ as the potential of tetrahedron $OA_2B_2C_2$ with density σ_2, $U_{t_3\sigma_2}^{(k)}$

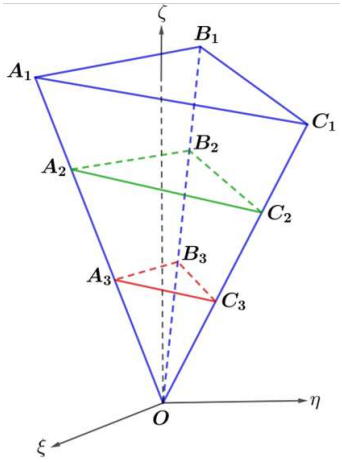


Fig. 5 Division of a tetrahedral element into three layers.

as the potential of tetrahedron $OA_3B_3C_3$ with density σ_2, and $U^{(k)}_{t_3\sigma_3}$ as the potential of tetrahedron $OA_3B_3C_3$ with density σ_3, the total potential of the tetrahedral element, considering the three densities, is given by Equation (29).

$$U^{(k)} = \sum_{q=1}^{2} \left(U^{(k)}_{t_q\sigma_q} - U^{(k)}_{t_{q+1}\sigma_q} \right) + U^{(k)}_{t_3\sigma_3}. \tag{29}$$

Based on the analytical model of the gravitational potential of the tetrahedral element Q_k, that is, $OA_1B_1C_1$, obtained by the Potential Series Expansion Method (PSEM) in Section (2.1), and knowing the proportionality ratios between the similar tetrahedra in Figure 5, h_1 and h_2, given by Equation (30),

$$\frac{V_{A_2B_2C_2O}}{V_{A_1B_1C_1O}} = (h_1)^3 \quad \text{and} \quad \frac{V_{A_3B_3C_3O}}{V_{A_1B_1C_1O}} = (h_2)^3 \tag{30}$$

we calculate the potentials of the tetrahedra $A_2B_2C_2O$ and $A_3B_3C_3O$, expressed by Equations (31) and (32).

$$U^{(k)}_{t_2\sigma_p} = U^{(k)}_0 + (h_1)\, U^{(k)}_1 + (h_1)^2 U^{(k)}_2 + \ldots + (h_1)^i U^{(k)}_i, \tag{31}$$

$$U^{(k)}_{t_3\sigma_q} = U^{(k)}_0 + (h_2)\, U^{(k)}_1 + (h_2)^2 U^{(k)}_2 + \ldots + (h_2)^i U^{(k)}_i, \tag{32}$$

where σ_p and σ_q are the densities established initially, with $p = 1, 2$ and $q = 2, 3$, and where $U_1, U_2, \ldots, U_i$ are given by Equation (27). Therefore, the model of the

gravitational potential around an asteroid with a three-layer structure is given by Equation (33).

$$U = \sum_{k=1}^{n} U^{(k)} = \sum_{k=1}^{n} \left[\sum_{q=1}^{2} \left(U^{(k)}_{t_q \sigma_q} - U^{(k)}_{t_{q+1} \sigma_q} \right) + U^{(k)}_{t_3 \sigma_3} \right]. \tag{33}$$

Finally, it is worth noting that the analytical model of the gravitational field around an asteroid can also be obtained using the potential series expansion method by considering the body as composed of several concentric internal layers, depending on its physical characteristics and composition.

3 Equations of motion and equilibrium points

In this work, only the disturbance generated by the gravitational field is taken into account, leaving other disturbances such as solar radiation pressure and the effects of solar gravitation for a later study.

3.1 Equations of motion

We adopted the coordinate system fixed to the asteroid for all equations. Therefore, to obtain the gravitational potentials of the asteroids studied in this work, the PSEM series potential expansion method was used in conjunction with the decomposition of the asteroid into tetrahedral elements [18, 20, 23]; that is, we used Equation (19).

As mentioned previously, the asteroid considered here has a rotational speed only about the z-axis. Assuming this uniform rotation, the equations of motion of a particle orbiting the asteroid [24, 25] are expressed in the form of Equation (34).

$$\ddot{\mathbf{r}} + 2\left(\omega \times \dot{\mathbf{r}}\right) + \omega \times \left(\omega \times \mathbf{r}\right) = -\frac{\partial U}{\partial \mathbf{r}}. \tag{34}$$

with $\mathbf{r}$ being the position vector of the particle, $\dot{\mathbf{r}}$ the first, and $\ddot{\mathbf{r}}$ the second temporal derivatives relative to the system fixed to the asteroid, $\boldsymbol{\omega}$ the angular velocity vector of the asteroid relative to the inertial system, and U the gravitational potential of the asteroid, given by Equation (27). We can then define the effective potential function using Equation (35).

$$V\left(\mathrm{r}\right) = -\frac{1}{2}\left(\omega \times \mathrm{r}\right) \cdot \left(\omega \times \mathrm{r}\right) + U\left(\mathrm{r}\right) \ , \tag{35}$$

making it possible to rewrite Equation (34) as Equation (36)

$$\ddot{\mathbf{r}} + 2\left(\omega \times \dot{\mathbf{r}}\right) + \frac{\partial V}{\partial \mathbf{r}} = 0 \ . \tag{36}$$

In this work, we consider small bodies in uniform rotation and assume that $\omega = \omega\,\mathbf{e}_z$, where $\mathbf{e}_z$ is the unit vector along the z-axis, which simplifies Equation (36).

3.2 Determination of equilibrium points

The Hamiltonian function, as given in Hu and Scheeres [26], can be expressed by Equation (37).

$$H=\frac{1}{2}\dot{\mathbf{r}}\cdot\dot{\mathbf{r}}+\mathrm{V}\left(\mathbf{r}\right)\ , \tag{37}$$

and because ω is time-invariant, we can conclude that H will also be time-invariant, and it is called the Jacobi constant. Redefining $H = C$, the region that prohibits particle circulation is given by $V(r) > C$, while the region that allows the particle to circulate satisfies $V(r) < C$. Lastly, the condition $V(r) = C$ implies that the particle is stationary with respect to the system fixed to the asteroid, defining the zero-velocity surfaces. Therefore, equilibrium points are the critical points of the effective potential $V(\mathbf{r})$, that is, those satisfying $\nabla V(x, y, z) = 0$, and thus must satisfy Equation (38).

$$\frac{\partial \mathrm{V}\left(x,y,z\right)}{\partial x}=\frac{\partial \mathrm{V}\left(x,y,z\right)}{\partial y}=\frac{\partial \mathrm{V}\left(x,y,z\right)}{\partial z}=0. \tag{38}$$

These algebraic equations were solved numerically using *Mathematica*, determining the coordinates of the equilibrium points, designated by $(x_E, y_E, z_E)^{\mathrm{T}}$. It should be noted that the positions, stabilities, and topological classification of the equilibrium points vary depending on the shape and angular velocity of the asteroid.

To study their stability, the effective potential is expanded in a Taylor series in the neighborhood of each equilibrium point, allowing the linearization of the equations of motion and the derivation of the associated characteristic equation $P(\lambda) = 0$, given by Equation (39). The roots λ, also called eigenvalues, provide fundamental information about the stability of the equilibrium points.

$$P\left(\lambda\right)=\begin{vmatrix}\lambda^2+V_{xx} & -2\omega\lambda+V_{xy} & V_{xz}\\ 2\omega\lambda+V_{xy} & \lambda^2+V_{yy} & V_{yz}\\ V_{xz} & V_{yz} & \lambda^2+V_{zz}\end{vmatrix}=0. \tag{39}$$

In Equation (39), we have the partial derivatives given by Equation (40).

$$\begin{aligned}\mathrm{V}_{xx}&=\left(\frac{\partial^2\mathrm{V}}{\partial x^2}\right)_E \quad \mathrm{V}_{xy}=\left(\frac{\partial^2\mathrm{V}}{\partial x\partial y}\right)_E\\ \mathrm{V}_{yy}&=\left(\frac{\partial^2\mathrm{V}}{\partial y^2}\right)_E \quad \mathrm{V}_{yz}=\left(\frac{\partial^2\mathrm{V}}{\partial y\partial z}\right)_E\ ,\\ \mathrm{V}_{zz}&=\left(\frac{\partial^2\mathrm{V}}{\partial z^2}\right)_E \quad \mathrm{V}_{xz}=\left(\frac{\partial^2\mathrm{V}}{\partial x\partial z}\right)_E\end{aligned} \tag{40}$$

Here $V_{pq} = \left(\frac{\partial^2 V}{\partial p\, \partial q}\right)_E$, for $p, q \in \{x, y, z\}$, denotes the value of the second derivative evaluated at the equilibrium point.

4 Results of Gravitational Field Modeling

For the asteroids investigated in this work, we developed the gravitational potential up to degree 11, achieving excellent accuracy and a substantial reduction in computational cost for computing the potential, determining equilibrium points, and performing orbital stability analyses.

This detailed analytical approach was similarly applied to other asteroids, including (87) Sylvia, (101955) Bennu, and (25143) Itokawa, yielding consistent and reliable results.

In Table 1, we present the coefficients of the potential U as defined in Eq. (26) (and expanded in Eq. (28)) for the several asteroids studied in this paper. We limit those shown in Table 1 to the fourth degree for readability purposes.

4.1 Gravitational Field Modeling Results with Uniform Density

We used the PSEM to model the gravitational fields of four asteroids: (87) Sylvia, (101955) Bennu, (25143) Itokawa, and (99942) Apophis, assuming homogeneous density. We matched the polyhedral shape model to the body's center of mass and primary inertia axes, then estimated the mass using the measured volume and a reference density. The gravitational potential was computed on a grid of 1.002×10^6 points using PSEM, and compared to the classical polyhedral result [8]. We define the relative error by $\mathrm{RE} = (U - U_W)/U_W$. In all cases the equilibrium points and their stability as determined by PSEM agree with published values, confirming the method's accuracy. Moreover, PSEM yields dramatic computational speed-ups over the classical method, as shown below.

4.1.1 Asteroid (87) Sylvia

As a representative example, we studied (87) Sylvia using an 800-face DAMIT model [27–29]. With $\rho = 1.373$,g/cm^3 [30] (mass 1.47×10^{19},kg) and spin period 5.184,h [28]. The PSEM potential, expanded to 14th order, exhibits high fidelity compared to the classical polyhedral solution. Figure 6, top-left panel, shows the relative error between the PSEM and classical polyhedral potentials Werner [8], evaluated at 10^6 field points spanning radial distances from the surface outward. The error remains below 0.05% beyond the physical radius and drops rapidly as the distance increases, demonstrating the convergence and accuracy of the PSEM in the exterior region. The narrow band of higher error near the body surface reflects the intrinsic challenge of approximating strong potential gradients via truncated series, but the solution remains smooth and continuous.

Table 2 compares CPU performance on a 3.60 GHz processor: the classical polyhedral method required 2m16.606s, while the PSEM at order 14 computed the same

Table 1 Coefficients $U_l^{i,j,k}$ for the asteroids investigated in this work. These values complete the potential U shown in Eq. (26).

i	j	k	Sylvia	Bennu	Apophis	Itokawa
$l=0$						
0	0	0	0.98056	5.2011×10^{-9}	3.5440×10^{-9}	2.3522×10^{-9}
$l=1$						
0	1	0	-1.3690×10^{-14}	7.5380×10^{-22}	1.8634×10^{-22}	-6.4698×10^{-26}
1	0	0	-2.0766×10^{-14}	4.6749×10^{-22}	2.1021×10^{-22}	4.5123×10^{-25}
0	0	1	-2.8815×10^{-14}	3.4913×10^{-22}	-2.1454×10^{-22}	6.3890×10^{-26}
$l=2$						
2	0	0	2948.4	1.2080×10^{-11}	1.5696×10^{-11}	3.6746×10^{-11}
0	2	0	-1166.5	6.1635×10^{-12}	-5.3039×10^{-12}	-1.6444×10^{-11}
0	0	2	-1781.9	-1.8244×10^{-11}	-1.0392×10^{-11}	-2.0303×10^{-11}
1	0	1	3.5324×10^{-12}	1.3254×10^{-22}	-6.8185×10^{-23}	4.0458×10^{-26}
1	1	0	4.2022×10^{-14}	1.6543×10^{-22}	7.0602×10^{-23}	3.8206×10^{-27}
0	1	1	-2.5420×10^{-12}	1.0520×10^{-22}	4.6107×10^{-23}	1.2444×10^{-26}
$l=3$						
0	0	3	7584.3	4.8710×10^{-13}	1.1519×10^{-12}	9.7640×10^{-13}
0	3	0	38358	5.1459×10^{-14}	1.5243×10^{-14}	-6.2762×10^{-13}
3	0	0	-37264	7.5378×10^{-14}	-2.0139×10^{-12}	1.9555×10^{-12}
0	1	2	80672	-2.4053×10^{-13}	-3.4625×10^{-13}	-4.1452×10^{-13}
1	0	2	80468	8.9255×10^{-13}	1.1004×10^{-12}	-1.8948×10^{-12}
2	0	1	2712.7	-1.0514×10^{-12}	-5.0704×10^{-12}	-3.9093×10^{-12}
1	2	0	31324	-1.1187×10^{-12}	4.9413×10^{-12}	-3.9716×10^{-12}
2	1	0	-1.9575×10^{5}	8.6152×10^{-14}	3.0052×10^{-13}	2.2974×10^{-12}
0	2	1	-25466	-4.0984×10^{-13}	1.6146×10^{-12}	9.8012×10^{-13}
1	1	1	42230	-1.1239×10^{-12}	-2.4424×10^{-12}	-1.2426×10^{-12}
$l=4$						
4	0	0	2.3302×10^{7}	3.1272×10^{-13}	6.9193×10^{-14}	1.0633×10^{-12}
0	0	4	1.4986×10^{7}	7.1983×10^{-13}	3.1608×10^{-14}	4.4015×10^{-13}
0	4	0	5.2473×10^{6}	2.0813×10^{-13}	3.8479×10^{-14}	3.7298×10^{-13}
0	3	1	4.9761×10^{6}	3.2060×10^{-13}	-1.1625×10^{-13}	1.0149×10^{-13}
3	1	0	4.2891×10^{7}	7.5015×10^{-13}	4.7171×10^{-14}	1.8354×10^{-13}
1	0	3	3.5367×10^{6}	-1.9650×10^{-13}	-1.7965×10^{-13}	5.4087×10^{-13}
0	2	2	9.2059×10^{6}	-1.8457×10^{-12}	-2.6832×10^{-15}	7.5046×10^{-13}
2	0	2	-9.9125×10^{7}	-2.4733×10^{-12}	-1.8696×10^{-13}	-3.3913×10^{-12}
0	1	3	-1.6840×10^{7}	-2.7570×10^{-13}	-4.4775×10^{-14}	7.6151×10^{-14}
3	0	1	-7.1046×10^{6}	1.4700×10^{-13}	2.1472×10^{-13}	-7.2687×10^{-13}
1	3	0	-1.7690×10^{7}	-6.7910×10^{-13}	-8.2821×10^{-14}	-1.8129×10^{-13}
2	2	0	-4.0690×10^{7}	5.9694×10^{-13}	-2.2819×10^{-13}	-2.9883×10^{-12}
2	1	1	3.5592×10^{7}	-1.3470×10^{-13}	4.8308×10^{-13}	-5.3294×10^{-13}
1	2	1	1.0704×10^{7}	1.4848×10^{-13}	-1.0521×10^{-13}	5.5798×10^{-13}
1	1	2	-7.5603×10^{7}	-2.1314×10^{-13}	1.0695×10^{-13}	-6.7487×10^{-15}

field in only 16.979s, yielding a speed-up of approximately ~ 2.5 times. We located four equilibrium points (Table 3, Fig 7, top-left panel); linear stability analysis (Table 4) indicates that E_1 and E_3 are saddle–center–center (Case 2), while E_2 and E_4 are sink–source–center (Case 5) according to the classification of Jiang et al. [31], Wang et al. [32].

4.1.2 Other asteroids

The other bodies follow the same pattern. For (101955) Bennu we used a 12288-face model (PDS) with $\rho = 1.25$,g/cm^3 ($m = 7.79 \times 10^{10}$,kg, spin 4.297,h). The PSEM (order 11) again yields small relative errors beyond the surface (Fig. 6, top-right panel) and a ~ 21.1 times speed-up: Table 2 shows classical polyhedral method 23m28.575s vs. PSEM 1m6.632s. Eight equilibrium points are found (Table 3, Fig 7, top-right panel); we find E_1, E_3, E_5, E_7 in Case 2, E_2, E_4, E_8 in Case 5, and E_6 in Case 1 (linearly stable) Jiang et al. [31], Wang et al. [32]. Similarly, (99942) Apophis (3996 vertices, $\rho = 1.75$,g/cm^3, spin 30.40,h) and (25143) Itokawa (12192 faces, $\rho = 1.98$,g/cm^3) show the same trends: PSEM (order 10 for Apophis and 9 for Itokawa) produces errors below 0,01% beyond the surface (Figs. 6, bottom panels) and yields ~ 8.2 times and ~ 27.1 times speed-ups, respectively (Table 2). Apophis has four (two in Case 2 and two in Case 1, the latter being linearly stable) and Itokawa has four equilibrium points (two in Case 2 and two in Case 5). In all cases, the PSEM-derived potentials and resulting dynamical properties agree with classical methods, while greatly reducing computation time. These results demonstrate PSEM's robustness: it reproduces the known equilibrium structure of each asteroid while reducing computational cost by orders of magnitude compared to the traditional polyhedral approach. This validates PSEM as an efficient and accurate tool for modeling the gravitational fields of irregular asteroids.

Table 2 Execution time for calculating the gravitational potential on a grid of 1,002,000 points close to the target using a Pentium 3.60 GHz CPU.

Target	Faces	Werner [8]	This work
(87) Sylvia	800	2m16.606s	0m54.929s
(101955) Bennu	12288	23m28.575s	1m6.632s
(99942) Apophis	3996	9m58.786s	1m12.890s
(25143) Itokawa	12192	29m14.496s	1m4.760s
(21) Lutetia	2962	74m30.86s	4m25.98s

4.2 Asteroid (21) Lutetia: Three-Layer Density Model

Asteroid (21) Lutetia is an M-type main-belt asteroid with a mean diameter of approximately 98 km and a bulk density near 3.4 g/cm^3 [33, 34], suggesting a differentiated interior. Following the internal structure proposed by Aljbaae et al. [35], we adopted a three-layer concentric model consisting of an iron-rich core (7.4 g/cm^3), a basaltic mantle (3.8 g/cm^3), and a crust (3.2 g/cm^3), scaled to preserve the total mass of the homogeneous case, as shown in Fig. 8. The polyhedral shape model used (2962 triangular facets) was obtained from the PDS database and reoriented along its principal axes, assuming a rotation period of 8.16827 h [36]. This stratified configuration was modeled using PSEM, enabling efficient evaluation of the gravitational field and potential under realistic interior assumptions.

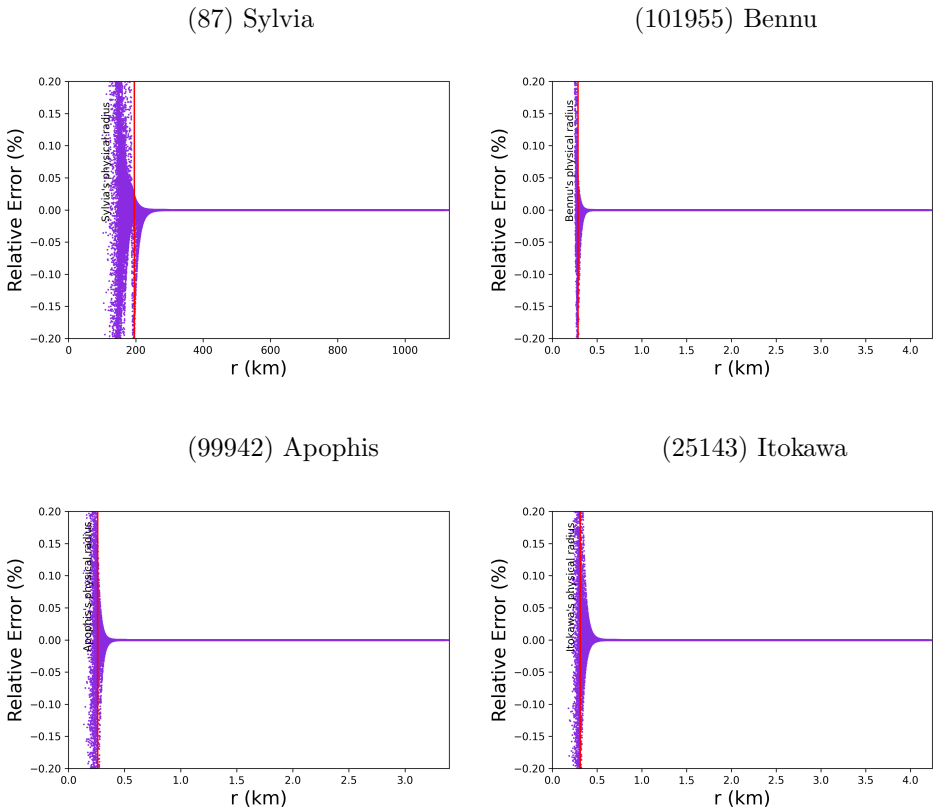


Fig. 6 Relative error of the gravitational potential U_{PSEM} with respect to the classical polyhedral method (U_W)

We applied the PSEM, using similarity scaling for each concentric tetrahedral shell (Eqs. 31, 32) so that the total potential is given by Eq. 33. Figure 9, left panel shows the relative error between the PSEM solution and the classical polyhedral method of Werner [8], evaluated at 10^6 field points. As seen, the error remains below 0.2% across the entire domain and converges rapidly to zero with distance.

The results of the system analysis are shown in Table 3 and in the right panel of Fig. 9. To study the stability of the four outer equilibrium points, we looked at their eigenvalues listed in Table 4. Points E_1 and E_2 have one pair of real eigenvalues and two pairs of imaginary ones (known as Case 2, saddle–center type), which makes them unstable. On the other hand, points E_3 and E_4 have three pairs of imaginary eigenvalues (Case 1, center-type), meaning they are considered linearly stable [31, 32].

5 Conclusion

The main objective of this work was to develop a method to model the external gravitational field of several asteroids. We used the Potential Series Expansion Method

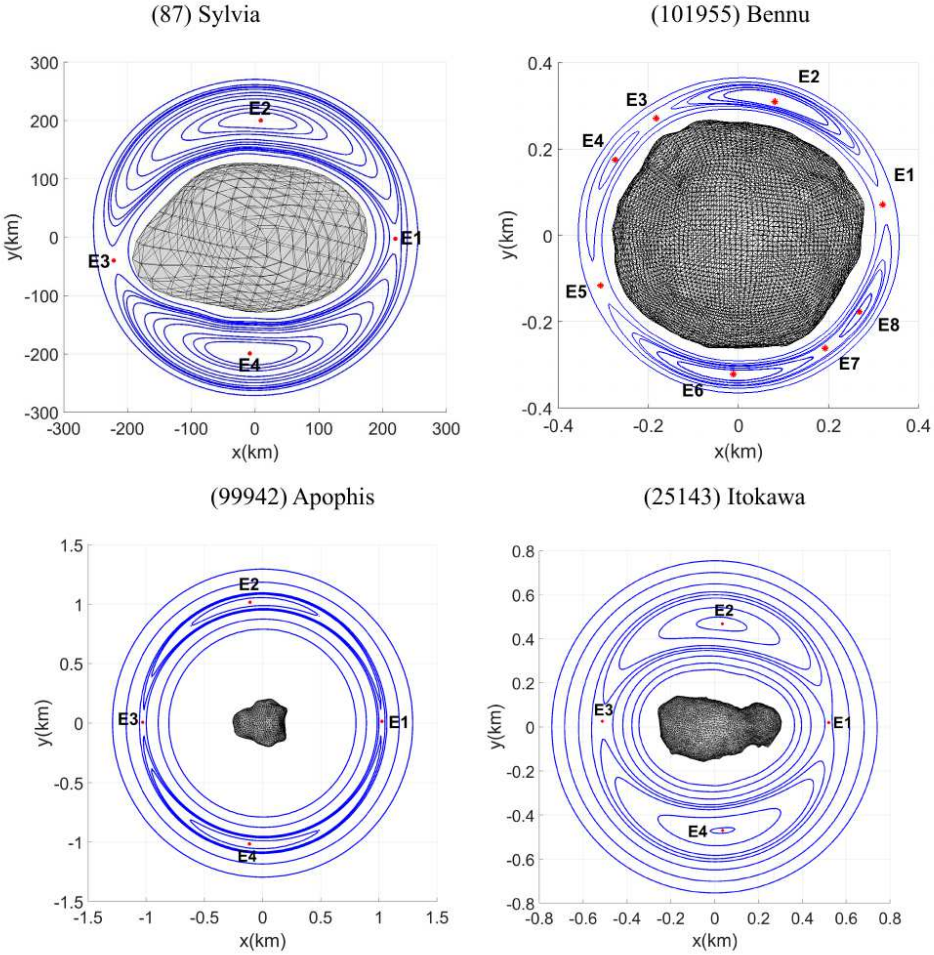


Fig. 7 Zero-velocity curves and equilibrium points of the target

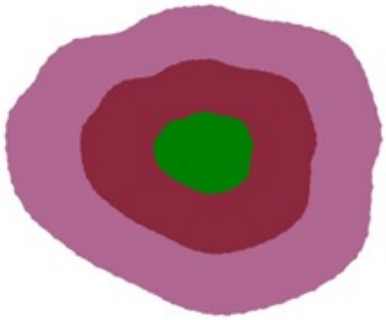


Fig. 8 Relative error between PSEM and classical polyhedral solution for (21) Lutetia. The red vertical line indicates the physical radius of the asteroid.

Table 3 Position of the equilibrium points (in km) outside the target, using the potential series expansion method, and their relative errors (RE) compared to the classical polyhedral method.

	x	y	z	$\|RE\|(\%)$
(87) Sylvia				
E_1	220.197	-3.299	-1.037	0.011
E_2	6.188	200.590	0.231	0.006
E_3	-221.755	-41.648	-0.141	0.073
E_4	-8.681	-199.301	-1.012	0.034
(101955) Bennu				
E_1	0.320	0.071	-0.001	0.123
E_2	0.081	0.310	0.001	0.002
E_3	-0.183	0.271	-0.000	0.087
E_4	-0.274	0.174	-0.002	0.035
E_5	-0.307	-0.116	-0.002	0.032
E_6	-0.011	-0.321	-0.002	0.034
E_7	0.192	-0.261	-0.001	0.031
E_8	0.268	-0.178	-0.001	0.027
(99942) Apophis				
E_1	1.028	-0.014	-0.001	0.008
E_2	-0.108	1.017	0.000	0.008
E_3	-1.029	0.005	-0.001	0.007
E_4	-0.114	-1.017	0.000	0.008
(25143) Itokawa				
E_1	0.521	0.020	-0.009	0.001
E_2	0.035	0.468	0.002	0.020
E_3	-0.512	0.025	-0.005	0.008
E_4	0.037	-0.470	0.002	0.007
(21) Lutetia				
E_1	137.064	8.380	0.081	-0.001
E_2	-138.101	6.538	0.042	-0.001
E_3	-8.661	134.098	0.035	-0.001
E_4	-14.479	-134.127	0.083	-0.001

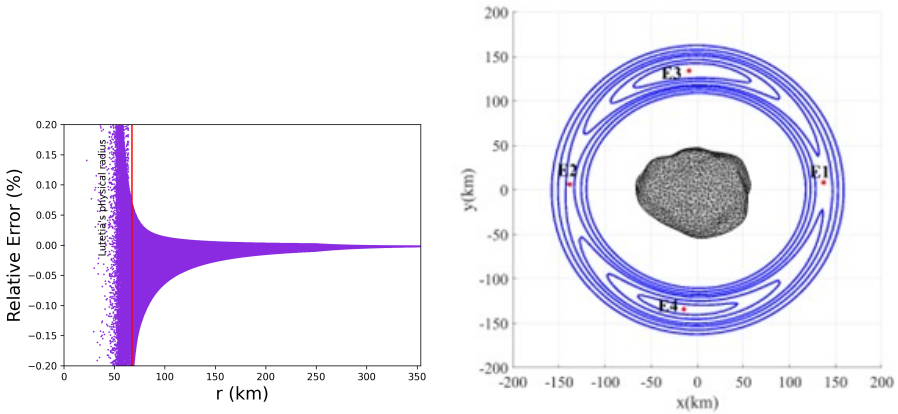


Fig. 9 Left panel: Comparison of gravitational modeling results for asteroid (21) Lutetia. **Right panel:** Locations of the equilibrium points computed using the PSEM model.

Table 4 Eigenvalues of the equilibrium points around asteroid (87) Sylvia.

(87) Sylvia				
$\times 10^{-4}$	E_1	E_2	E_3	E_4
λ_1	2.536	3.413i	3.376	3.456i
λ_2	-2.536	-3.413i	-3.376	-3.456i
λ_3	3.903i	-0.965 + 2.538i	4.201i	-1.277 + 2.645i
λ_4	-3.903i	-0.965 - 2.538i	-4.201i	-1.277 - 2.645i
λ_5	3.725i	0.965 + 2.538i	4.052i	1.277 + 2.645i
λ_6	-3.725i	0.965 - 2.538i	-4.052i	1.277 - 2.645i
(101955) Bennu				
$\times 10^{-4}$	E_1	E_2	E_3	E_4
λ_1	2.168	4.436i	1.999	4.569i
λ_2	-2.168	-4.436i	-1.999	-4.569i
λ_3	4.082i	0.713 + 2.676i	3.975i	0.755 + 2.575i
λ_4	-4.082i	0.713 - 2.676i	-3.975i	0.755 - 2.575i
λ_5	4.585i	-0.713 + 2.676i	4.602i	-0.755 + 2.575i
λ_6	-4.585i	-0.713 - 2.676i	-4.602i	-0.755 - 2.575i
	E_5	E_6	E_7	E_8
λ_1	1.937	2.012i	1.830	4.416i
λ_2	-1.937	-2.012i	-1.830	-4.416i
λ_3	3.889i	3.033i	4.018i	0.695 + 2.688i
λ_4	-3.889i	-3.033i	-4.018i	0.695 - 2.688i
λ_5	4.650i	4.443i	4.494i	-0.695 + 2.688i
λ_6	-4.650i	-4.443i	-4.494i	-0.695 - 2.688i
(99942) Apophis				
$\times 10^{-5}$	E_1	E_2	E_3	E_4
λ_1	-0.830	-1.123i	-1.224	-1.116i
λ_2	0.830	1.123i	1.224	1.116i
λ_3	-5.762i	-5.622i	-5.785i	-5.624i
λ_4	5.762i	5.622i	5.785i	5.624i
λ_5	-5.779i	-5.749i	-5.827i	-5.748i
λ_6	5.779i	5.749i	5.827i	5.748i
(25143) Itokawa				
$\times 10^{-4}$	E_1	E_2	E_3	E_4
λ_1	1.165	1.446i	0.928	1.453i
λ_2	-1.165	-1.446i	-0.928	-1.453i
λ_3	1.606i	-0.497 + 1.127i	1.565i	-0.418 + 1.091i
λ_4	-1.606i	-0.497 - 1.127i	-1.565i	-0.418 - 1.091i
λ_5	1.708i	0.497 + 1.127i	1.598i	0.418 + 1.091i
λ_6	-1.708i	0.497 - 1.127i	-1.598i	0.418 - 1.091i
(21) Lutetia				
$\times 10^{-3}$	E_1	E_2	E_3	E_4
λ_1	0.0675	0.0941	0.0958i	0.0746i
λ_2	-0.0675	-0.0941	-0.0958i	-0.0746i
λ_3	0.218i	0.223i	0.189i	0.196i
λ_4	-0.218i	-0.223i	-0.189i	-0.196i
λ_5	0.220i	0.225i	0.215i	0.217i
λ_6	-0.220i	-0.225i	-0.215i	-0.217i

(PSEM) to model the small celestial bodies. It consists of applying the gravitational structure using a shaped polyhedral source associated with a series potential expansion, similarly to the spherical harmonics method. In this way, we detailed such an approach to evaluate the external gravitational potential of a polyhedron with constant density, as well as that of a body composed of three concentric layers with distinct densities. This method has the advantage of explicitly displaying the gravitational field, facilitating algebraic manipulation to obtain the acceleration components and compute the velocity increments, while significantly reducing CPU time requirements and maintaining accuracy at a very acceptable level. These capabilities were demonstrated for the asteroids (101955) Bennu, (99942) Apophis, (25143) Itokawa, and (87) Sylvia assuming constant density, but also for the asteroid (21) Lutetia, assuming a structure formed by three concentric layers with distinct densities. Furthermore, we determined the equilibrium points, analyzed their stability, investigated the zero-velocity planes, and calculated the relative errors between the gravitational field modeled by PSEM and those obtained using both the classical polyhedral method of Tsoulis and Petrovic and the mass concentration method, demonstrating the computational efficiency of PSEM in modeling the gravitational potential of irregularly shaped bodies.

The Potential Series Expansion Method (PSEM) not only maintains a high level of accuracy in modeling the gravitational potential of irregularly shaped celestial bodies but also reduces computational processing time by up to 98% compared to the classical polyhedral method developed by Tsoulis, making it a highly efficient and effective tool for such analyses. It is important to note that PSEM is valid and uniformly convergent outside the Brillouin sphere, the smallest sphere enclosing the entire mass of the body. In this region, the method provides reliable and accurate approximations of the gravitational field. However, as with spherical harmonic models, the series may diverge within the Brillouin sphere, limiting its applicability closer to the body's surface. Despite this limitation, the uniform convergence outside the sphere ensures its robustness for exterior applications, particularly in scenarios relevant to spacecraft dynamics and mission planning.

The analytical expressions derived in this paper can be very useful during the early stages of mission design, where orbits must remain stable over long time spans. This capability allows the extension of mission duration by minimizing the use of control systems to keep the spacecraft on its nominal trajectory. The search for stable orbits is computationally intensive, making computational efficiency a critical factor. Furthermore, simple analytical expressions such as those derived here are particularly useful for spacecraft control systems in situations where, due to communication limitations (e.g., occultation, temporal constraints, etc.), orbital correction calculations must be performed onboard with very limited computational resources. Consequently, the analytical expressions derived in this paper can be valuable at multiple stages of missions aimed at exploring small celestial bodies.

Furthermore, it is worth highlighting that, when the internal structure of an asteroid is known, for example, in cases of non-constant specific mass, our method allows the analysis of modeling effects for bodies composed of several concentric layers.

Author Contributions

M. L. Mota initiated the work and developed the mathematical framework. S. Aljbaae was responsible for the programming aspect, utilizing Python and the SymPy library to implement the mathematical components. A. F. B. A. Prado supervised the project and validated the results. All authors reviewed and approved the final manuscript.

Data Availability

This study is primarily analytical and methodological in nature. The manuscript presents the complete mathematical framework, derivations, and implementation methodology required to reproduce the polynomial representation of the gravitational potential of irregular celestial bodies. No new observational datasets, experimental measurements, or standalone numerical databases were generated specifically for this work.

The asteroid shape models used in this study were obtained from previously published publicly available sources cited throughout the manuscript. Therefore, a dedicated data repository is not applicable to this study.

Appendix A Integral of a Polynomial over a Rectangular Tetrahedron

Due to the importance of this integral in deriving the gravitational potential model presented in this work, its full derivation is provided below.

The Beta and Gamma functions are defined by Equations (A1) and (A2), respectively:

$$\beta\left(n_1+1, n_2+1\right) = \int_0^1 x^{n_1}(1-x)^{n_2} dx \tag{A1}$$

$$\Gamma\left(n+1\right) = \int_0^\infty e^{-x} x^n dx = n! \tag{A2}$$

and are related through Equation (A3).

$$\beta\left(m,n\right) = \frac{\Gamma\left(m\right)\Gamma\left(n\right)}{\Gamma\left(m+n\right)} = \frac{(m-1)!\ \ (n-1)!}{(m+n-1)!}. \tag{A3}$$

Therefore, the integral of the function $f(x,y,z) = x^{n_1}\, y^{n_2}\, z^{n_3}$ over the rectangular tetrahedron W, with vertices located at the points $O(0,0,0)$, $V_1(1,0,0)$, $V_2(0,1,0)$, and $V_3(0,0,1)$, is expressed by Equation (A4).

$$
\begin{aligned}
I = \iiint_W x^{n_1} y^{n_2} z^{n_3} dx\, dy\, dz &= \int_0^1 \int_0^{1-z} \int_0^{1-z-y} x^{n_1} y^{n_2} z^{n_3} dx\, dy\, dz \\
&= \frac{1}{n_1+1} \int_0^1 \int_0^{1-z} (1-z-y)^{n_1+1} y^{n_2} z^{n_3} dy\, dz \\
&= \frac{1}{n_1+1} \int_0^1 \int_0^{1-z} (1-z)^{n_1+1} \left(1 - \frac{y}{1-z}\right)^{n_1+1} y^{n_2} z^{n_3} dy\, dz
\end{aligned} \tag{A4}
$$

Defining $Y = \frac{y}{1-z}$, we obtain $y = (1-z)Y$. Therefore, $\frac{dy}{dY} = (1-z)$, which, when substituted into Equation (A4), yields Equation (A5).

$$
I = \frac{1}{n_1+1} \int_0^1 \int_0^1 (1-z)^{n_1+1} (1-Y)^{n_1+1} (1-z)^{n_2} Y^{n_2} z^{n_3} (1-z)\, dY\, dz. \tag{A5}
$$

By algebraically manipulating Equation (A5), we obtain Equation (A6).

$$
I = \frac{1}{n_1+1} \int_0^1 \int_0^1 (1-Y)^{n_1+1} Y^{n_2} (1-z)^{(n_1+n_2+2)} z^{n_3} dY\, dz, \tag{A6}
$$

which can be rewritten using Equation (A7)

$$
I = \frac{1}{n_1+1} \int_0^1 \beta\left(n_2+1, n_1+2\right) (1-z)^{(n_1+n_2+2)} z^{n_3} dz \tag{A7}
$$

$$
I = \frac{\beta\left(n_2+1, n_1+2\right)}{n_1+1} \int_0^1 (1-z)^{(n_1+n_2+2)} z^{n_3} dz \tag{A8}
$$

In turn, Equation (A8) subsequently yields Equations (A9) and (A10):

$$
I = \frac{\beta\left(n_2+1, n_1+2\right)}{n_1+1} \beta\left(n_3+1, n_1+n_2+3\right) \tag{A9}
$$

$$
I = \frac{1}{(n_1+1)} \frac{n_2!\,(n_1+1)!}{(n_1+n_2+2)!} \frac{n_3!\,(n_1+n_2+2)!}{(n_1+n_2+n_3+3)!}. \tag{A10}
$$

Therefore, the integral of the polynomial function $f(x,y,z) = x^{n_1}\, y^{n_2}\, z^{n_3}$ over the rectangular tetrahedron W is given by Equation (A11).

$$I = \iiint_W x^{n_1} y^{n_2} z^{n_3} dx\, dy\, dz = \frac{n_1!\; n_2!\; n_3!}{(n_1 + n_2 + n_3 + 3)!}. \tag{A11}$$

References

[1] MacMillan, W.D.: The Theory of the Potential. (MacMillan: Theoretical Mechanics), (1930). https://books.google.com.br/books?id=-PEgAAAAMAAJ

[2] Kaula, W.M.: Theory of Satellite Geodesy. Applications of Satellites to Geodesy, (1966)

[3] Heiskanen, W.A., Moritz, H.: Physical Geodesy, (1967)

[4] Balmino, G.: Gravitational Potential Harmonics from the Shape of an Homogeneous Body. Celestial Mechanics and Dynamical Astronomy **60**(3), 331–364 (1994) https://doi.org/10.1007/BF00691901

[5] Roithmayr, C.M.: Contributions of Spherical Harmonics to Gravitational Moment. AIAA Journal **57**(10), 4291–4299 (2019) https://doi.org/10.2514/1.J057227

[6] Casotto, S.: Representation of the External Potential of a Solid Body within its Brillouin Sphere. In: AAS/Division for Planetary Sciences Meeting Abstracts #32. AAS/Division for Planetary Sciences Meeting Abstracts, vol. 32, pp. 65–29 (2000)

[7] Werner, R.A., Scheeres, D.J.: Exterior gravitation of a polyhedron derived and compared with harmonic and mascon gravitation representations of asteroid 4769 castalia. Celestial Mechanics and Dynamical Astronomy **65**(3), 313–344 (1996) https://doi.org/10.1007/BF00053511

[8] Werner, R.A.: The Gravitational Potential of a Homogeneous Polyhedron or Don't Cut Corners. Celestial Mechanics and Dynamical Astronomy **59**(3), 253–278 (1994) https://doi.org/10.1007/BF00692875

[9] Scheeres, D.: Orbital motion in strongly perturbed environments. Orbital Motion in Strongly Perturbed Environments, by Scheeres, Daniel J. ISBN: 978-3-642-03255-4. Berlin: Springer, 2012 (2012) https://doi.org/10.1007/978-3-642-03256-1

[10] Tsoulis, D.: Analytical computation of the full gravity tensor of a homogeneous arbitrarily shaped polyhedral source using line integrals. Geophysics **77**, 1 (2012) https://doi.org/10.1190/geo2010-0334.1

[11] D'Urso, M., Lieto, D.: Gravitational fields of polyhedral bodies with 3d polynomial density contrast. Surveys in Geophysics **45**, 1–89 (2024) https://doi.org/10.1007/s10712-023-09822-8

[12] Geissler, P., Petit, J.-M., Durda, D.D., Greenberg, R., Bottke, W., Nolan, M., Moore, J.: Erosion and Ejecta Reaccretion on 243 Ida and Its Moon. *icarus* **120**(1), 140–157 (1996) https://doi.org/10.1006/icar.1996.0042

[13] Chanut, T.G.G., Aljbaae, S., Carruba, V.: Mascon gravitation model using a shaped polyhedral source. Monthly Notices of the Royal Astronomical Society **450**(4), 3742–3749 (2015) https://doi.org/10.1093/mnras/stv845

[14] Aljbaae, S., Sanchez, D.M., Prado, A.F.B.A., Souchay, J., Terra, M.O., Negri, R.B., Marchi, L.O.: First approximation for spacecraft motion relative to (99942) apophis. Romanian Astronomical Journal **31**(3), 241–264 (2021)

[15] Rossi, A., Marzari, F., Farinella, P.: Orbit propagation with high-resolution shape models of asteroids. Planetary and Space Science **47**(11-12), 1397–1405 (1999) https://doi.org/10.1016/S0032-0633(99)00059-7

[16] Izzo, D., Gómez, P.: Geodesy of irregular small bodies via neural density fields. Communications Engineering **1**, 48 (2022) https://doi.org/10.1038/s44172-022-00050-3

[17] Martin, J., Schaub, H.: Physics-informed neural networks for gravity field modeling of small bodies. Celestial Mechanics and Dynamical Astronomy **134**, 46 (2022) https://doi.org/10.1007/s10569-022-10101-8

[18] Mota, M.L.: Modelo do campo gravitacional de um corpo com distribuição de massa irregular utilizando o método da expansão do potencial em série e determinaçao de seus coeficientes dos harmônicos esféricos. PhD thesis, INPE, São José dos Campos (2017)

[19] Werner, R.A., Scheeres, D.J.: Exterior gravitation of a polyhedron derived and compared with harmonic and mascon gravitation representations of asteroid 4769 castalia. Celestial Mechanics and Dynamical Astronomy **65**(3), 313–344 (1997) https://doi.org/10.1007/BF00053511

[20] Mota, M.L., Aljbaae, S., Prado, A.F.B.A.: The potential series expansion method: application to the asteroid (87) sylvia. European Physical Journal Special Topics **232**(18-19), 2961–2966 (2023) https://doi.org/10.1140/epjs/s11734-023-01026-w

[21] Kellogg, O.D.: Foundations of Potential Theory. Die Grundlehren der mathematischen Wissenschaften in Einzeldarstellungen, (1953). https://books.google.com.br/books?id=TxlfQi46CvEC

[22] Lien, S.-l., Kajiya, J.T.: A symbolic method for calculating the integral properties

of arbitrary nonconvex polyhedra. IEEE Computer Graphics and Applications **4**(10), 35–42 (1984) https://doi.org/10.1109/MCG.1984.6429334

[23] Mota, M.L., Rocco, E.M.: Equilibrium points stability analysis for the asteroid 21 lutetia. In: Journal of Physics: Conference Series, vol. 1365, p. 012007 (2019). https://doi.org/10.1088/1742-6596/1365/1/012007

[24] Greenwood, D.T.: Principles of Dynamics. Prentice-Hall international series in dynamics, (1988). https://books.google.com.br/books?id=j_RQAAAAMAAJ

[25] Scheeres, D.J., Ostro, S.J., Hudson, R.S., Werner, R.A.: Orbits Close to Asteroid 4769 Castalia. *icarus* **121**(1), 67–87 (1996) https://doi.org/10.1006/icar.1996.0072

[26] Hu, W.-D., Scheeres, D.J.: Periodic Orbits in Rotating Second Degree and Order Gravity Fields. *Chin. J. Astron. Astrophys.* **8**(1), 108–118 (2008) https://doi.org/10.1088/1009-9271/8/1/12

[27] Durech, J., Sidorin, V., Kaasalainen, M.: DAMIT: a database of asteroid models. *Astron. Astrophys.* **513**, 46 (2010) https://doi.org/10.1051/0004-6361/200912693

[28] Marchis, F., Kaasalainen, M., Hom, E.F.Y., Berthier, J., Enriquez, J., Hestroffer, D., Le Mignant, D., de Pater, I.: Shape, size and multiplicity of main-belt asteroids. I. Keck Adaptive Optics survey. *icarus* **185**, 39–63 (2006) https://doi.org/10.1016/j.icarus.2006.06.001

[29] Hanuš, J., Marchis, F., Ďurech, J.: Sizes of main-belt asteroids by combining shape models and Keck adaptive optics observations. *icarus* **226**, 1045–1057 (2013) https://doi.org/10.1016/j.icarus.2013.07.023 arXiv:1308.0446 [astro-ph.EP]

[30] Berthier, J., Vachier, F., Marchis, F., Ďurech, J., Carry, B.: Physical and dynamical properties of the main belt triple Asteroid (87) Sylvia. *icarus* **239**, 118–130 (2014) https://doi.org/10.1016/j.icarus.2014.05.046 arXiv:1407.1292 [astro-ph.EP]

[31] Jiang, Y., Baoyin, H., Wang, X., Li, H.: Stability and Motion around Equilibrium Points in the Rotating Plane-Symmetric Potential Field. arXiv e-prints, 1403–1967 (2014) https://doi.org/10.48550/arXiv.1403.1967 arXiv:1403.1967 [astro-ph.EP]

[32] Wang, X., Jiang, Y., Gong, S.: Analysis of the potential field and equilibrium points of irregular-shaped minor celestial bodies. *Astrophys. Space Sci.* **353**(1), 105–121 (2014) https://doi.org/10.1007/s10509-014-2022-8 arXiv:1403.5025 [astro-ph.EP]

[33] Coradini, A., Capaccioni, F., Erard, S., Arnold, G., De Sanctis, M.C., Filacchione, G., Tosi, F., Barucci, M.A., Capria, M.T., Ammannito, E., Grassi, D., Piccioni, G., Giuppi, S., Bellucci, G., Benkhoff, J., Bibring, J.P., Blanco, A., Blecka, M., Bockelee-Morvan, D., Carraro, F., Carlson, R., Carsenty, U., Cerroni, P., Colangeli, L., Combes, M., Combi, M., Crovisier, J., Drossart, P., Encrenaz, E.T., Federico, C., Fink, U., Fonti, S., Giacomini, L., Ip, W.H., Jaumann, R., Kuehrt, E., Langevin, Y., Magni, G., McCord, T., Mennella, V., Mottola, S., Neukum, G., Orofino, V., Palumbo, P., Schade, U., Schmitt, B., Taylor, F., Tiphene, D., Tozzi, G.: The Surface Composition and Temperature of Asteroid 21 Lutetia As Observed by Rosetta/VIRTIS. Science **334**(6055), 492 (2011) https://doi.org/10.1126/science.1204062

[34] Weiss, B.P., Elkins-Tanton, L.T., Antonietta Barucci, M., Sierks, H., Snodgrass, C., Vincent, J.-B., Marchi, S., Weissman, P.R., Pätzold, M., Richter, I., Fulchignoni, M., Binzel, R.P., Schulz, R.: Possible evidence for partial differentiation of asteroid Lutetia from Rosetta. *planss* **66**(1), 137–146 (2012) https://doi.org/10.1016/j.pss.2011.09.012

[35] Aljbaae, S., Chanut, T.G.G., Carruba, V., Souchay, J., Prado, A.F.B.A., Amarante, A.: The dynamical environment of asteroid 21 Lutetia according to different internal models. *Mon. Not. Roy. Astron. Soc.* **464**, 3552–3560 (2017) https://doi.org/10.1093/mnras/stw2619 arXiv:1610.02338 [astro-ph.EP]

[36] Carry, B., Kaasalainen, M., Leyrat, C., Merline, W.J., Drummond, J.D., Conrad, A., Weaver, H.A., Tamblyn, P.M., Chapman, C.R., Dumas, C., Colas, F., Christou, J.C., Dotto, E., Perna, D., Fornasier, S., Bernasconi, L., Behrend, R., Vachier, F., Kryszczynska, A., Polinska, M., Fulchignoni, M., Roy, R., Naves, R., Poncy, R., Wiggins, P.: Physical properties of the ESA Rosetta target asteroid (21) Lutetia. II. Shape and flyby geometry. *Astron. Astrophys.* **523**, 94 (2010) https://doi.org/10.1051/0004-6361/201015074 arXiv:1005.5356 [astro-ph.EP]